VISIT…

ELASTOHYDRODYNAMIC LUBRICATION

Herbert S. Cheng

INTRODUCTION

Elastohydrodynamic lubrication (EHL) applies to conditions where surface deformation and hydrodynamic action both play important roles. The most prominent example of EHL is the Hertzian contact in rolling element bearings, gears, and cams where surface deformation often exceeds the mean film thickness.

In elastohydrodynamic contacts, lubrication effectiveness is often measured by the average film thickness separating the asperities between two surfaces. Good lubrication performance is usually achieved when the mean separation approaches or exceeds three times the composite rms value of surface roughness. In this full-film region, overall performance can usually be predicted by EHL theories considering smooth boundaries. While full-film EHL theories are useful in predicting performance, partial-film EHL (Figure 1) relations are required in forecasting conditions for failure by pitting, scuffing, or wear.

Effects of surface deformation in sliding journal and thrust bearings can also be regarded as EHL problems and will be discussed briefly. Finally, application of EHL theories in roller and ball bearings, spur gears, helical gears, and cams will be reviewed.

FULL-FILM EHL

After two decades of intensive efforts, characteristics of full-film EHL are now reasonably well understood. The principal features were first revealed in two-dimensional analyses for line contacts. Later, three-dimensional analyses showed additional features in point or elliptical contacts.

Line Contacts

Line contact geometry applies to cases which correspond to two cylinders in contact: rolling-element bearings, uncrowned spur and helical gears, etc. Most EHL analyses have used this geometry both because it is easiest to analyze and because it reveals basic features common in more complicated contacts.

Film Thickness

Classical lubrication theories for rigid rollers are of interest to show their inadequacy in predicting film thickness for EHL contacts. Two rigid rollers are equivalent to a rigid roller on a flat plate, shown in Figure 2. The lubricant transported at any point along the film is

$$\left(\frac{u_1 + u_2}{2}\right) h - \frac{h^3}{12\mu}\left(\frac{dp}{dx}\right) \qquad (1)$$

where p, h, u_1, u_2, and μ are pressure, film thickness, surface velocity of roller 1 and 2, and viscosity, respectively.

Let the lubricant flow rate be 1/2 $(u_1 + u_2)h^*$, where h^* is the gap where dp/dx is zero. Continuity of flow gives

$$\frac{dp}{dx} = 6\mu(u_1 + u_2)\left(\frac{h - h^*}{h^3}\right) \qquad (2)$$

Copyright © 1983 CRC Press LLC

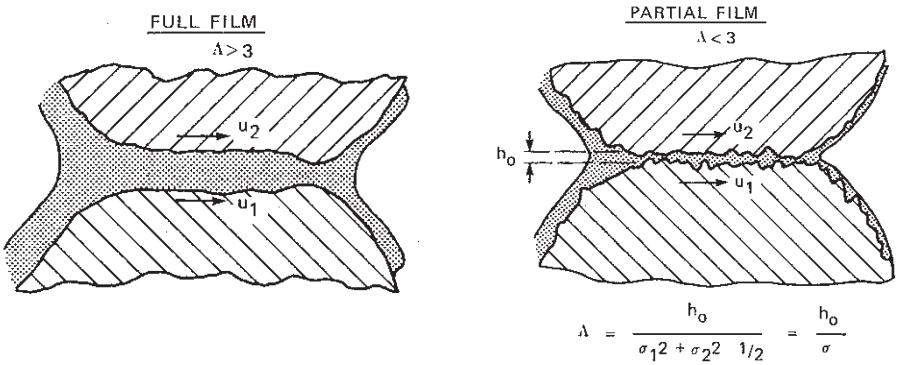

FIGURE 1. Full- and partial-film EHL contacts.

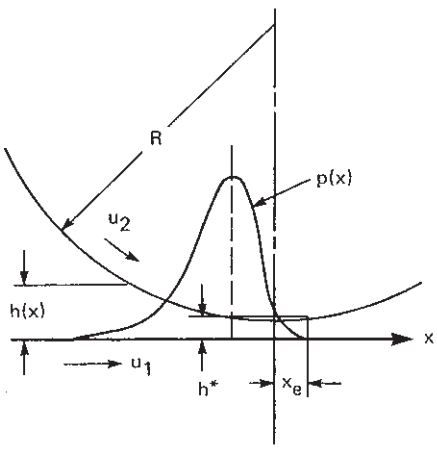

FIGURE 2. Lubrication of rigid roller on flat plate.

The boundary conditions are

$$p = 0 \text{ at } x = -\infty$$

$$p = 0, \frac{dp}{dx} = 0; h = h^* \text{ at } x = x_e$$

On the left side of h*, dp/dx is positive, resulting in a hydrodynamic pumping action. On the right side of h*, dp/dx is negative, resulting in a sealing action. By prescribing h*, one can solve Equation 2 for the pressure distribution, and hence the load and film thickness relationship.

After Martin[1] showed that this simple theory could not adequately predict a lubricating film for rolling contacts, many believed that pressure-viscosity dependence could account for a greater film thickness. Including the exponential relation $\mu = \mu_o e^{\alpha p}$ in Equation 2, one obtains:

$$\frac{1}{e^{\alpha p}} \frac{dp}{dx} = 6\mu_o(u_1 + u_2) \frac{h - h^*}{h^3} \quad (3)$$

Copyright © 1983 CRC Press LLC

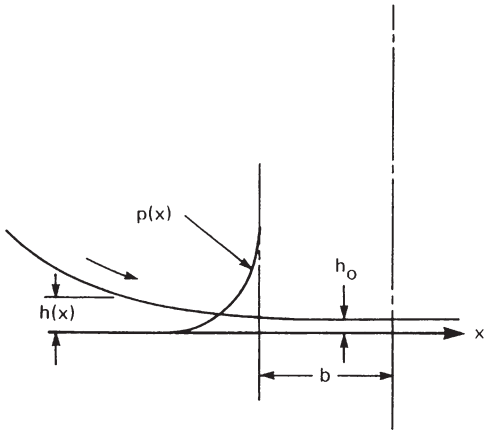

FIGURE 3. Inlet geometry of Grubin-lype EHL line contact.

where μ_o is the ambient viscosity and α the pressure-viscosity coefficient. By introducing a "reduced pressure" $q = (1 - e^{-\alpha p})/\alpha$, Equation 3 can be simplified to

$$\frac{dq}{dx} = 6\mu_o (u_1 + u_2) \frac{h - h^*}{h^3} \tag{4}$$

Equation 4 can be solved for q, which lead to p and the load capacity. Improvement in film thickness was still far from enough to suggest a full-film hypothesis.

Ertel-Grubin[2] provided the first convincing evidence of full-film EHL by solving Equation 4 for a Hertzian shape shown in Figure 3. They determined h_o, the inlet film thickness, for the reduced lubricant pressure q to reach $1/\alpha$ (or $p \rightarrow \infty$) at $x \rightarrow -b$, the entrance of the Hertzian conjunction. Once $e^{-\alpha p}$ approaches zero, μ becomes very large in the conjunction. A very minute change in conjunction film thickness would cause an enormous change in pressure. Therefore, for heavily loaded contacts, the gap in the conjunction is practically uniform. Equation 4 was solved using the Hertzian inlet film profile:

$$h(x) = h_o + \frac{4}{\Pi}\frac{w}{E}\left[|\bar{x}|\sqrt{\bar{x}^2 - 1} - \ln\left(|\bar{x}| + \sqrt{\bar{x}^2 - 1}\right)\right] \tag{5}$$

where $1/E = 1/2\,[(1 - \nu_1^2)/E\ 1 + (1 - \nu_2^2)/E_2]$ $\bar{x} = x/b$, and w = load per unit width. Empirical fitting yields the following equation which gives film thicknesses one or two orders of magnitude higher than rigid roller theories:

$$\frac{h_o}{R} = 1.95 \frac{(GU)^{8/11}}{(W)^{1/11}} \tag{6}$$

where $G = \alpha E$, $U = \mu_o u/ER$, $W = w/ER$, and $R = R_1R_2/(R_1 + R_2)$.

Ertel-Grubin's formula for predicting h_o holds well for a reasonably wide range of conditions. It becomes less accurate when $G < 1000$ (lubricant with a small pressure-viscosity dependence or material of low modulus) and when W becomes small ($<10^{-5}$). Solution for h_o for the full range of G from 0 to 5000 can be found in References 3, 4, and 5. Lubricant compressibility was included.

When U is very large, reduction of viscosity due to inlet shear heating requires solving the energy equation simultaneously with Equation 4 in the inlet region.[6-8] Results led to a

Copyright © 1983 CRC Press LLC

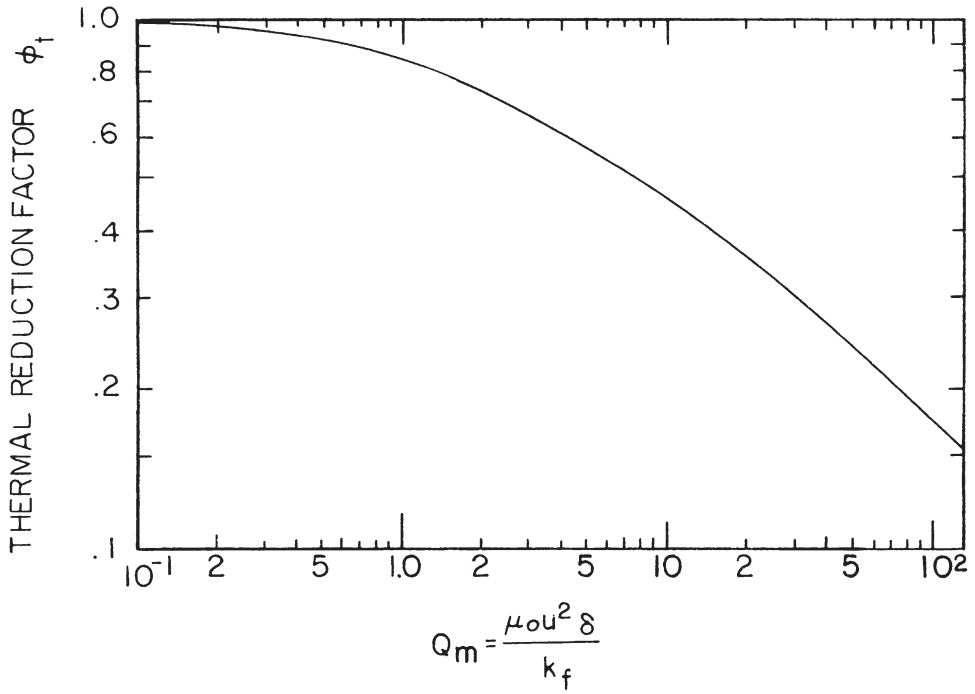

FIGURE 4. Thermal reduction factor, where Q_m = thermal parameter, μ_c = ambient lubricant viscosity, u = rolling velocity, T_o = ambient temperature, k_f = lubricant thermal conductivity, and δ = temperature viscosity coefficient in the empirical relation $\mu = \mu_o e^{-\delta}(T - T_o)$.

thermal reduction factor, ϕ_T, which can be multiplied by the Frtel-Grubin film thickness for the actual h_o. With ϕ_T, varying slightly with W and lubricant pressure G, Figure 4 gives a first approximation.[7]

Starvation introduced another reduction factor which is a function of the distance between the inlet film meniscus and the entrance edge of the Hertzian conjunction as indicated in Figure 5.[9,10] For rollers lubricated with an initial charge only, film thickness would be gradually reduced to about 0.71 of the fully flooded initial value.[10]

Measurements of film thickness in line contracts have been reviewed by Archard.[11] The first confirmation of Ertel-Grubin's film prediction was due to Crook,[12] who measured the capacitance between two discs. The second significant film measurement method was developed by Sibley and Orcutt[13] using X-ray techniques. Optical measurements were made by Wymer and Cameron.[14]

Film Shape and Pressure Distribution

For a detailed film thickness and pressure distribution, the following coupled Reynolds and deformation equations must be solved:

$$\frac{dp}{dx} = 6\mu(u_1 + u_2)\frac{h - h^*}{h^3} \tag{7}$$

$$h = h^* + \left(\frac{x^2 - x^{*2}}{2R}\right) - \frac{4}{\pi E}\int_{-\infty}^{x^*} \ln\frac{|\xi - x|}{|\xi - x^*|}\, p(\xi)d\xi \tag{8}$$

where x* is the coordinate at which the lubricant film terminates. At x = x*, h = h*, dp/dx = 0.

Copyright © 1983 CRC Press LLC

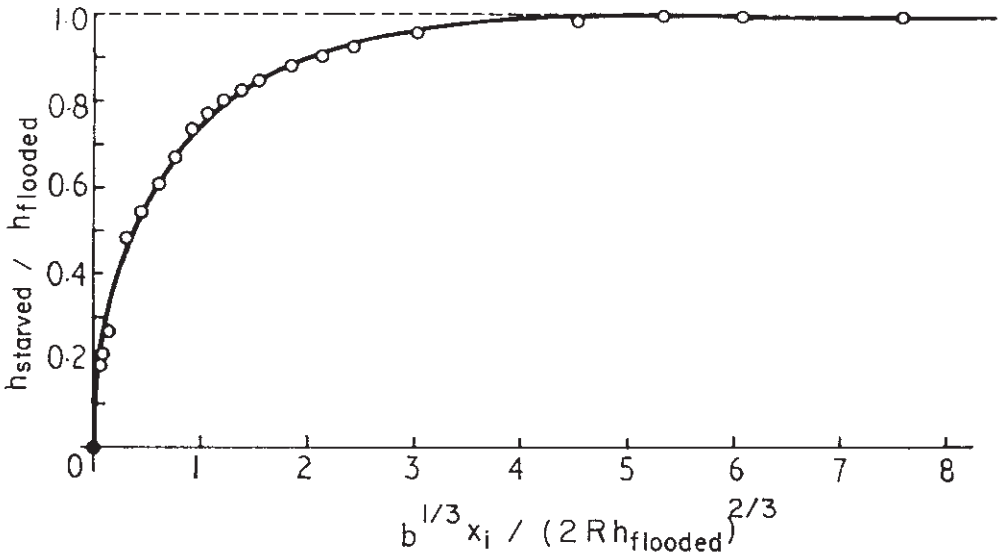

FIGURE 5. Effect of starved inlet boundary on film thickness, where b = half Hertzian width, x_1 = distance from the inlet oil meniscus to the inlet edge of Hertzian boundary, R = effective radius $R_1R_2/(R_1 + R_2)$, $h_{starved}$ = starved film thickness, and $h_{flooded}$ = flooded film thickness. The circle points are derived from the computer solution by Orcutt and Cheng.[83]

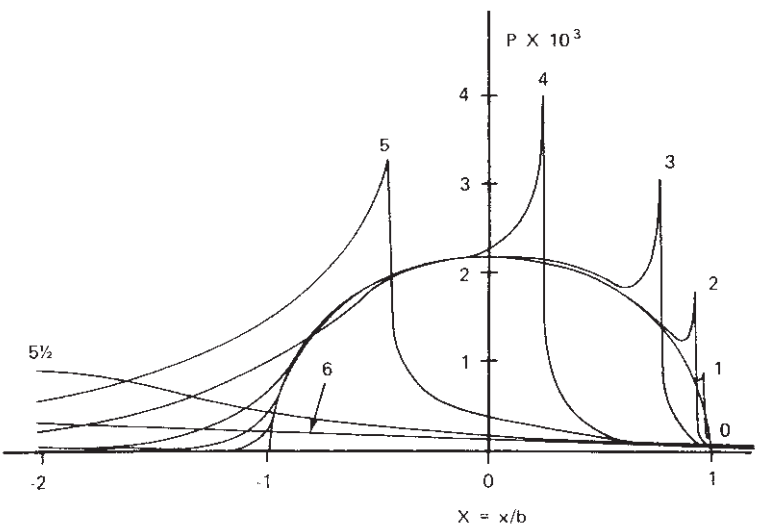

FIGURE 6. Pressure distributions for a compressible lubricant, where W = 3 × 10^{-5}, G = 5000, U = (0) 0 (dry contact), (1) 10^{-13}, (2) 10^{-12}, (3) 10^{-11}, (4) 10^{-10},(5) 10^{-9}, ($5^1/_2$) $10^{-8.5}$, and (6) 10^{-8} (for definition of W, G, and U, see Equation 6).

The first full EHL numerical solution revealed a sharp pressure spike accompanied by a film constriction at the exit, as shown in Figure 6.[15] As speed decreases or load increases, the pressure spike moves further towards the exit and eventually disappears for very heavily loaded contacts.[17] Similar features were found in later isothermal solutions.[18-20]

Inlet and central film thickness obtained in Reference 16 agrees well with the Ertel-Grubin solution. Minimum film thickness at the constriction was found to be approximately 70 to 75% of the central film thickness. This provided the following widely used minimum film thickness for line contacts.[21]

Copyright © 1983 CRC Press LLC

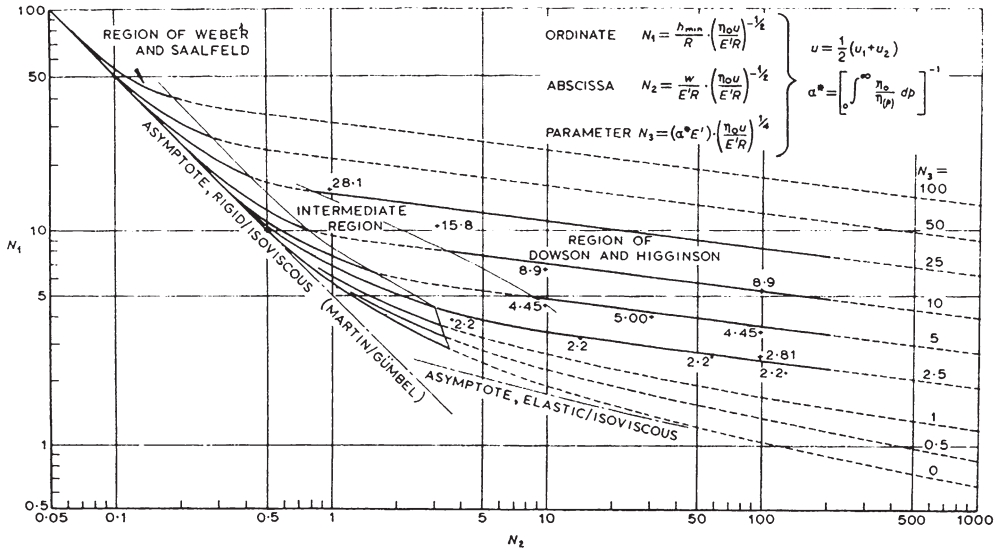

FIGURE 7. Survey diagram for incompressible and isothermal EHL.

$$\frac{h_{min}}{R} = 2.65 \frac{G^{0.54} U^{0.7}}{W^{0.13}} \qquad (9)$$

The exit construction was first seen experimentally in the circumferential film profile measured by the X-ray technique.[22] This was followed by optical interferometry.[14,22] While the measured nominal film shows good correlation with EHL theories, the measured ratio of minimum film to nominal film appears to be considerably smaller than 0.7 to 0.75, as predicted analytically. Film pressure measurements by means of a vapor-deposited manganin strip confirmed analytical predictions on effect of load on location of the pressure spike.[18,24,25]

Film Thickness Chart

Minimum film thickness of EHL line contacts may be determined from the Moes diagram[26] of Figure 7. Film thickness parameter h_{min}/R, speed parameter $\eta_o u/E'R$, load parameter, and lubricant parameter $\alpha^* E'$ are regrouped to form an implicit relation among only three independent parameters. Only one family of curves is needed to relate the film thickness parameter with the other two parameters over a wide range of loads, speeds, and lubricant parameters. Martin[1] results are an asymptote for the rigid/isoviscous case, and Herrebrugh[27] for the elastic/isoviscous case.

Point Contacts

Film Thickness

Figure 8 shows a point contact which is characterized by principal radii R_{x1}, R_{y1} for body 1 and R_{x2}, R_{y2} for body 2. In general, the principal planes containing R_{x1} and R_{x2} may not coincide: however, for most EHL contacts such as rolling bearings and gears, principal radii R_{x1} and R_{x2} do lie in the same plane. These surfaces can be convex, concave, or saddle-shape, depending on whether R_x and R_y are both positive, both negative, or mixed.

Ertel-Grubin type of analysis can also be carried out for spherical contacts with a circular conjection. Archard and Cowking[28] solved the two-dimensional Reynolds equation outside the circular conjunction region for a film thickness distribution compatible to the Hertzian solution for an unlubricated contact. An Ertel-Grubin type boundary condition, $q = 1/\alpha$, around the circumference of the circular conjunction gave:

Copyright © 1983 CRC Press LLC

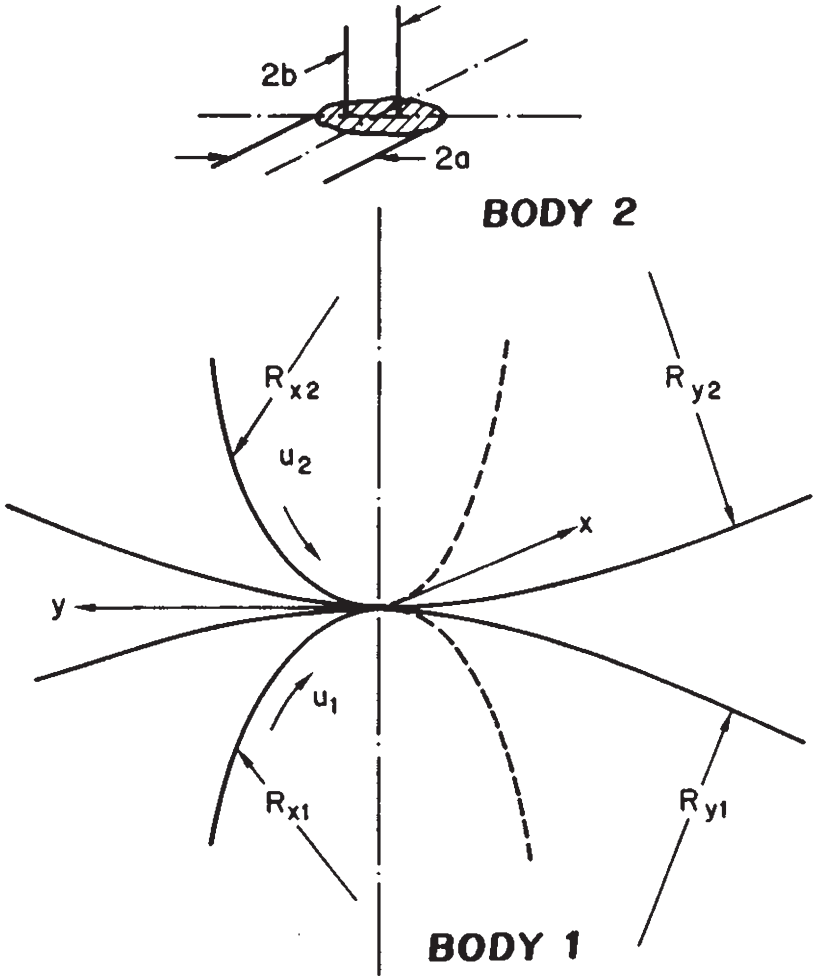

FIGURE 8. Geometry of an elliptical EHL contact.

$$\frac{h_o}{R} = 1.37\,(GU)^{0.74}\left(\frac{p_o}{E}\right)^{-0.22} \tag{10}$$

where p_o is the maximum Hertzian pressure. For point contacts with an elliptical conjunction, analytical solution is not feasible and numerical solutions have been obtained.[23,29] Results in Reference 29 gave:

$$\frac{h_o}{R} = C\,(GU)^{n_1}\left(\frac{p_o}{E}\right)^{n_2} \tag{11}$$

where C, n_1, n_2 in Table 1 are shown for four values of ellipticity ratios of the conjunction, a/b (b = semi-axis in the direction of motion, a = semi-axis normal to the motion).

Predictions of h_o using Equations 10 and 11 become inaccurate at high rolling speed where both inlet heating and starvation cause a reduction in h_o. While inlet heating for elliptical point contact has not been investigated, the thermal reduction factor for line contacts in Figure 4 may be applicable.

Copyright © 1983 CRC Press LLC

Table 1
VALUES OF C, n_1, AND n_2
FOR EQUATION 11

a/b	C	n_1	n_2
5	1.625	0.74	– 0.22
2	1.560	0.736	– 0.209
1	1.415	0.725	– 0.174
0.5	1.145	0.688	– 0.066

Full computer solutions for elliptical contacts were made for flooded as well as for starved contacts.[30] Film thickness formula for the flooded contacts appear as:

$$H_{c,F} = 2.69\ U^{0.67}\ G^{0.53}\ W^{-0.067}\ (1 - 0.61e^{-0.73k}) \qquad (12)$$

$$H_{min,F} = 3.63\ U^{0.68}\ G^{0.49}\ W^{-0.073}\ (1 - e^{-0.68k}) \qquad (13)$$

where $H_{c,F} = h_{c,F}/R_x$, $h_{c,F}$ = central film thickness for flooded contacts, $H_{min,F} = h_{min,F}/R_x$, $h_{min,F}$ = minimum film thickness for flooded contacts, k = elliptical parameter, k = 1.03 $(R_y/Rx)0.^{64}$, $R_x - R_{xl}R_{x2}/(R_{xl} + R_{x2})$, $R_y = R_{yl}R_{y2}/(R_{yl} + R_{y2})$, $W = w/ER_x^2$, w = total load, $U = \mu_o\ (u_1 + u_2)/2ER_x$, and $G = \alpha E$.

For the starved contacts, the formulas are

$$H_{c,s} = H_{c,F}\left(\frac{m - 1}{m^* - 1}\right)^{0.29} \qquad (14)$$

$$H_{min,s} = H_{min,F}\left(\frac{m - 1}{m^* - 1}\right)^{0.25} \qquad (15)$$

where subscript s refers to starved contacts, m is the distance of the inlet meniscus from the center of the contact, and m* is the inlet distance required for achieving flooded conditions; m* can be expressed as

$$m^* = 1 + 3.06\left[\left(\frac{R_x}{b}\right)^2 H_{c,F}\right]^{0.58} \qquad (16)$$

where b is the semiminor axis of the elliptical conjunction in the rolling direction.

In most starvation analyses, location of the inlet meniscus is not known beforehand and is dependent on lubricant supply rate and system configuration. Reduction in film thickness due to starvation in most ball bearings is considerably greater than from inlet healing.[31,32]

Optical techniques enabled extensive point-contact film thickness measurements and correlations with analysis.[33-36] Film thickness data by X-ray transmission[37] with crowned rollers showed a much stronger load dependence than that predicted by EHL analysis at maximum Hertzian pressures beyond 1 GPa (145,000 psi). This disagreement was explained by Gentle et al.[38] as possibly due to a combination of thermal and surface roughness effects. The point contact EHL film theory at extreme pressures [up to a maximum Hertzian pressure of 2 GPa (290,000 psi)l was validated by using a sapphire disk and tungsten carbide ball.[38] Film thickness measurements using tungsten carbide disks confirm EHL film theories for loads as high as 2.5 GPa (362,500 psi).[39]

Copyright © 1983 CRC Press LLC

Point Contact Film Shape and Pressure Distribution

Film shape in a circular point contact was experimentally revealed by the interferometric map between a highly polished steel ball and a transparent plate.[23,34,35,36,40] By identifying successive fringes, constant thickness contours can be mapped. The effect of speed on film shaped constriction which is very narrow and very close to the trailing edge. As speed increases or load decreases, the constriction becomes wider and less distinctive. Except for extremely low loads and high speeds, the minimum film thickness is found at the two sides rather than at the center of the trailing edge, and it is more sensitive to load variation than the minimum film thickness for a line contact. Analytical confirmation of the horseshoe-shaped constriction in a numerical solution of two-dimensional EHL equations[41] with a solid-like lubricant was followed by a series of full EHL solutions for circular and elliptical contacts[30,42] with a Newtonian lubricant.

Temperature

For a line contact, a detailed study of thermal effects required solution of the energy equation in the lubricant film considering heat generation by shearing and compressing the lubricant, heat convected away by the lubricant, and heat conducted into the solids.[43,44]

Film thickness level is influenced only by temperature rise in the inlet region discussed earlier; subsequent large temperature rise in the Hertzian conjunction has little influence. The predicted temperature field within the Hertzian conjunction depends strongly on the lubricant rheological model used in evaluating the heat generated by sliding. For a Newtonian model[44] for steel contacts with a maximum Hertzian pressure up to 0.5 GPa, the principal feature of exit film constriction and pressure peaks are unaltered when thermal effects are included. However, for loads higher than 0.5 GPa, the Newtonian lubricant model predicts a sliding frictional coefficient almost an order of magnitude higher than measured. Since practical sliding EHL contacts such as gears and cams involve pressures greater than 0.5 GPa, a non-Newtonian lubricant model is needed for the frictional heat. Successful non-Newtonian models are discussed in the next section.

Early measurement of surface temperature profiles were made with a platinium wire temperature transducer[24] at moderate loads. Later, an improved transducer[45,46] with a titanium wire deposited over a silica layer gave good results at much higher loads. While vapor-deposited probes are yet to perfected, a promising infrared technique was developed by Nagaraj et al.[47] for measuring the surface as well as film temperature in circular contacts. Figure 10 shows surface temperature along the center strip of the circular contact. The measured temperature show good agreement with that predicted from the Jaeger-Archard[48] formula.

Friction

In rolling and sliding EHD contacts, frictional force has two components: one due to rolling and the other due to slip between the surfaces. Except for nearly pure rolling conditions, sliding friction is always much larger than rolling friction. Basic features of sliding friction are revealed in Figure 11 by data from a two-disk machine.[49] In the low-slip region, friction increases linearly with slip. As slip increases, friction gradually tapers off in a nonlinear region where the stress is no longer governed by linear constitutive relations of the lubricant. In the high-slip region, friction decreases with slip because of thermal influence on lubricant properties at high-sliding speeds.

Low-Slip Friction

For low-slip frictions, sliding friction can be predicted from the Maxwell viscoelastic model. If equilibrium viscosity and shear modulus are used, however, predicted friction is much greater than measured. This disagreement led to the argument that the viscosity, when

Copyright © 1983 CRC Press LLC

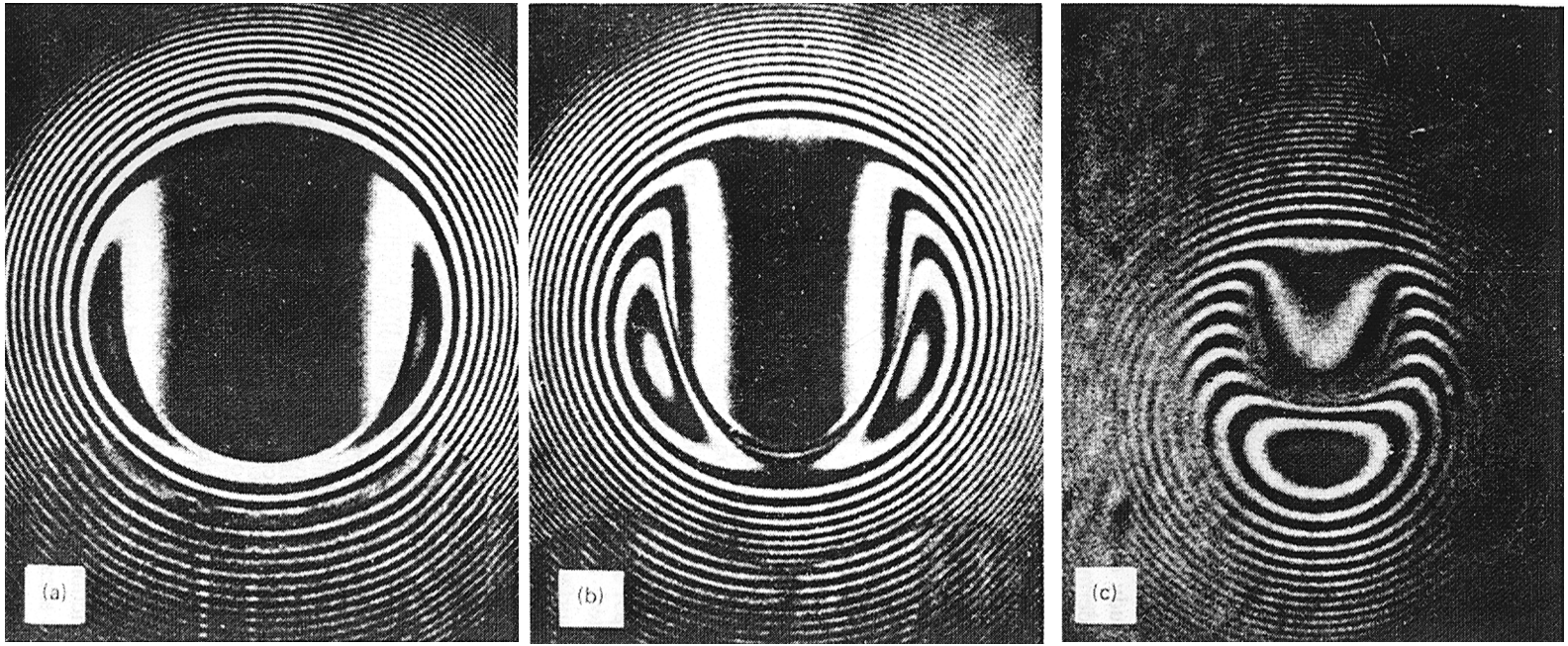

FIGURE 9. Effect of load and speed on film shape. (a) W = 10 lb, $U = \mu_o u/ER = 3 \times 10^{-11}$; (b) 10 lb, 1.8×10^{-10}; and (c) 5 lb, 1.5×10^{-9}.

Copyright © 1983 CRC Press LLC

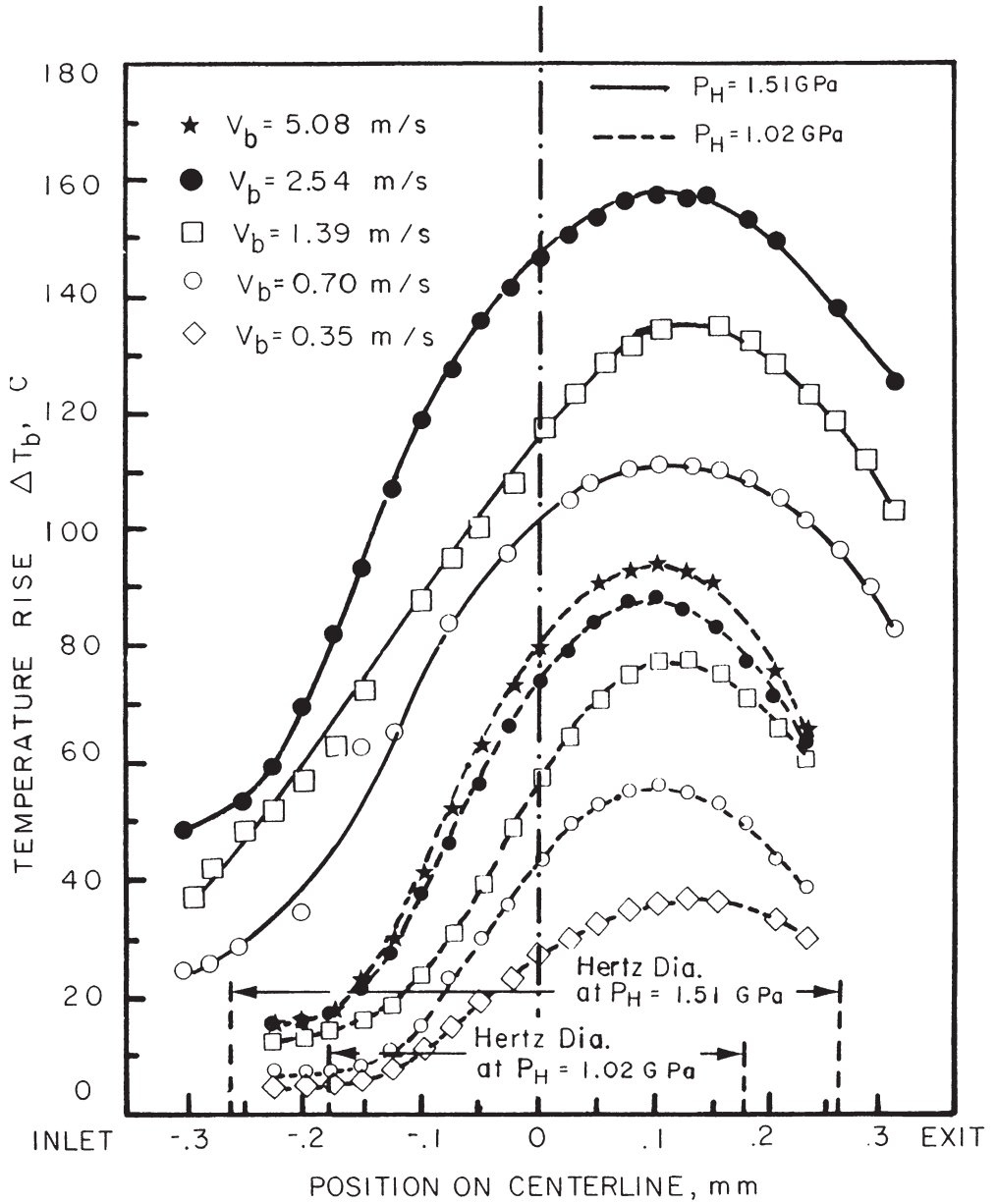

FIGURE 10. Ball surface temperature rise along centerline vs. speed. Smooth ball: 0.011 μm R_a, fluid NI (a naphthenic oil), T_{bath} = 40°C , $V_{sapphire}$ = 0, V_b = speed of ball surface, P_h = maximum Hertzian pressure, and T_b = ball surface temperature rise.

subjected to a sudden, higher pressure, cannot reach its equilibrium immediately. A time delay in the viscosity model[50] can account for the observed low friction[51] in the low-slip region even without considering shear elastic strain.

In a spin roll point contact, Johnson and Tevaariverk[52] have shown that oil under high-pressure and a short-transient time tends to deform more as an elastic solid than as a viscous liquid. However, values of shear modulus deduced from the low spin tests are still considerably lower than the known equilibrium shear modulus under high pressure.[53] They attributed this discrepancy in shear modulus to transient effects under a suddenly applied pressure.

Copyright © 1983 CRC Press LLC

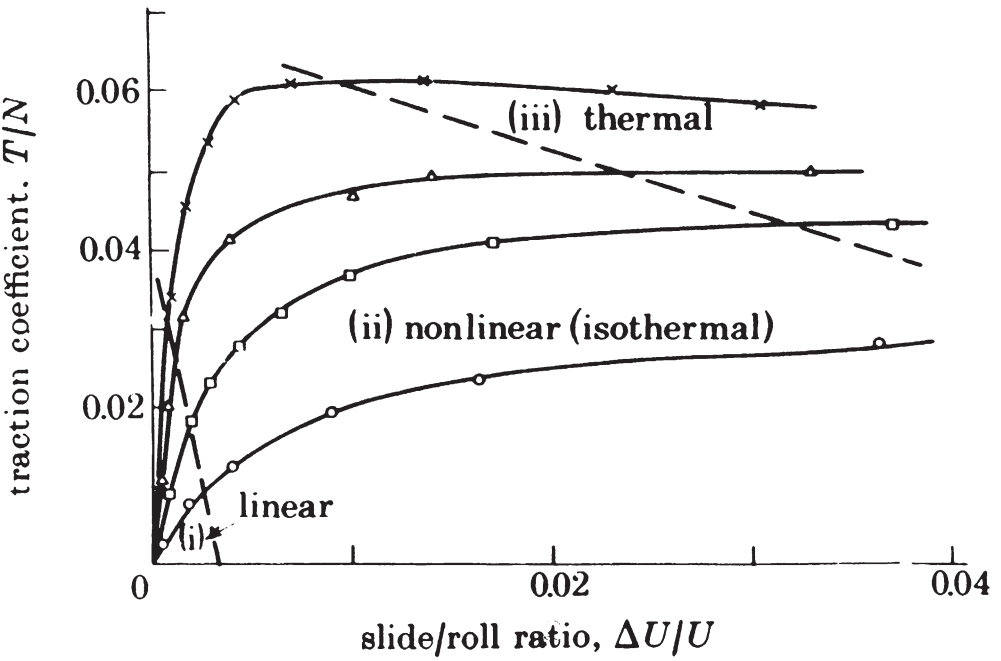

FIGURE 11. Typical traction curves measured on a two-disc machine in EHL line contact at varying mean contact pressure, p ; x, 1.03; Δ, 0.68; □, 0.51; ○, 0.40 GPa. (From Johnson, K. L. and Cameron, R., *Proc. Inst. Mech. Eng.,* 182, 307, 1967. With permission.)

Montrose et al.[54] developed perhaps the most complete and promising viscoelastic model to describe low-slip traction behavior. Shear elastic strain is considered in the same manner as the conventional viscoelastic theory. However, instead of actual local pressure, a fictive pressure accounts for the transient viscosity effects similar to that considered in Reference 50. The fictive pressure is determined from an exponentially decaying structural relaxation function.

High-Slip Friction

As sliding velocity increases, slope of the friction curve gradually decreases to zero, and in many cases becomes slightly negative at very high speed. Under these conditions, the fluid undergoes a large shear strain usually in the midplane of the lubricant film.

The Newtonian model was shown to be inadequate for predicting friction for heavily loaded contacts. It yields a friction force almost one order of magnitude higher than the measured value.[49] Non-Newtonian models for predicting friction in the high-slip region include a shear-dependent Ree-Eyring model,[55] a limiting shear liquid model,[56] a plastic solid model,[57] and a promising nonlinear viscous and plastic model.[52,58] This final model is capable of describing linear and nonlinear viscous, linear and nonlinear viscoelastic. as well as elastic plastic behavior in a single equation. Depicted in Figure 12, it is expressed as

$$\dot{\gamma} = \frac{1}{G}\frac{d\tau}{dt} + F(\tau) = \dot{\gamma}_e + \dot{\gamma}_e + \dot{\gamma}_v \tag{17}$$

$$F(\tau_e) = \left(\frac{\tau_o}{\eta}\right)\sinh\left(\frac{\tau_e}{\tau_o}\right) \tag{18}$$

where $\dot{\gamma}$ = total strain rate, $\dot{\gamma}_e$ = elastic strain rate, $\dot{\gamma}_v$ = viscous strain rate, τ_e = equivalent

Copyright © 1983 CRC Press LLC

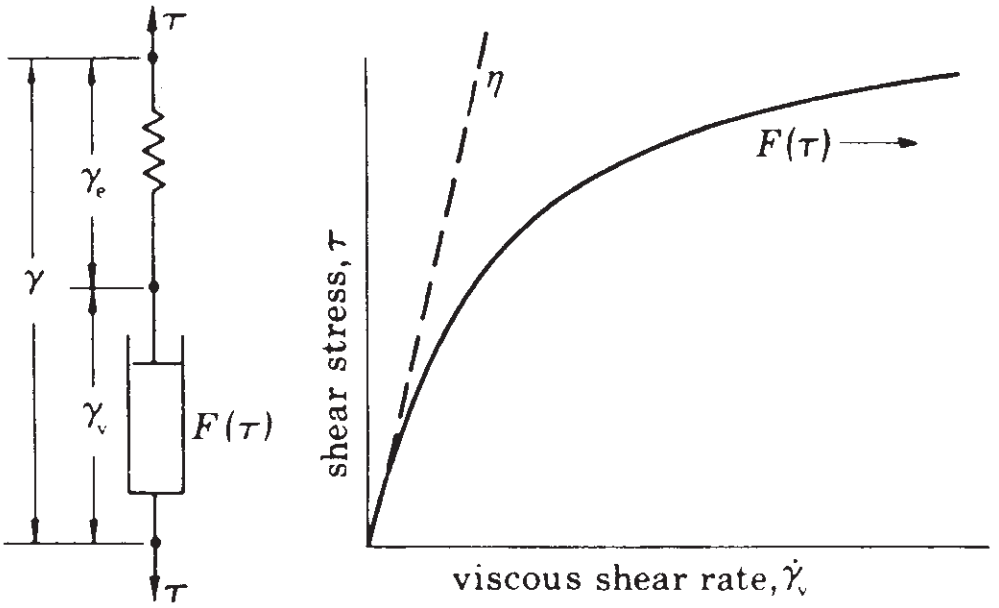

FIGURE 12. Nonlinear Maxwell fluid with zero-shear-rate viscosity and infinite-rate shear modulus G. F(τ) denotes the nonlinear viscous function.

stress = $(1/2\tau_{ij}\tau_{ij})^{1/2}$, τ_o = representative stress, a fluid property, η = viscosity, and G = shear modulus. τ_o, η, and G are fluid properties deduced from traction tests. Limited values are given for five oils.[52] A similar nonlinear viscous and plastic model introduced recently by Bair and Winer[58] used rheological constants from tests totally independent of any data from the EHL contact itself.

The Bair and Winer[58] model in dimensional form can be written as

$$\dot{\gamma} = \frac{1}{G_\infty}\frac{d\tau}{dt} - \frac{\tau_L}{\mu_o}\ln\left(1 - \frac{\tau}{\tau_L}\right) \tag{19}$$

In dimensionless form, it is

$$\hat{\dot{\gamma}} = \hat{\dot{\tau}} - \ln(1 - \hat{\tau}) \tag{20}$$

where

$$\hat{\dot{\gamma}} = \frac{\dot{\gamma}\mu_o}{\tau_L}$$

$$\hat{\dot{\tau}} = \frac{\mu_o}{\tau_L G_\infty}\frac{d\tau}{dt}$$

$$\hat{\tau} = \frac{\tau}{\tau_L}$$

Only three primary physical properties are required: low shear stress viscosity, μ_o, limiting elastic shear modulus, G_x, and limiting yield shear stress, τ_L, all as functions of temperature and pressure. The behavior of the dimensionless equation is shown in Figure 13. Agreement between theory and experiment is good.

Copyright © 1983 CRC Press LLC

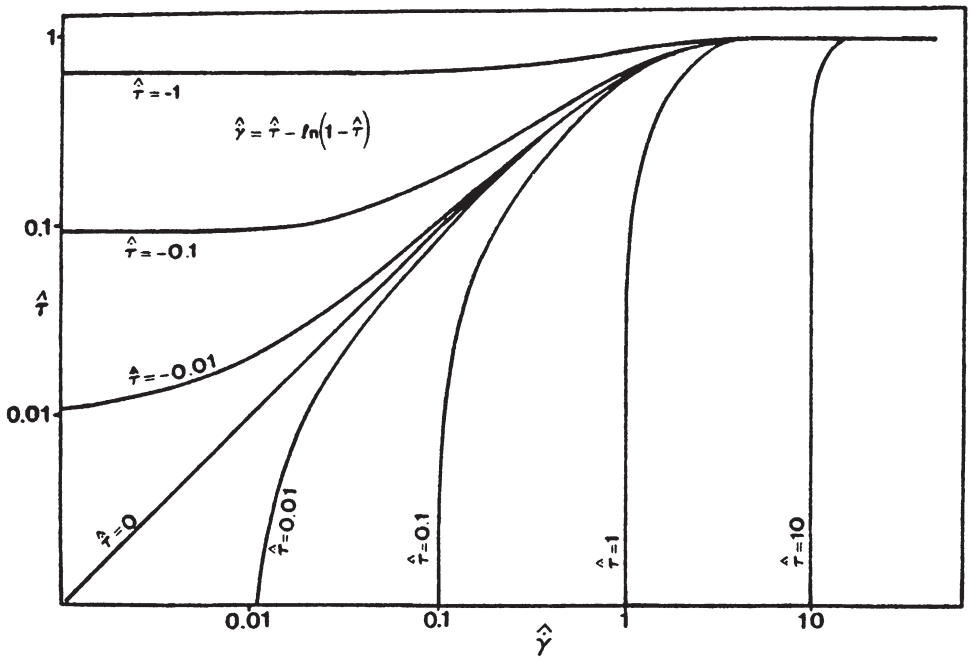

FIGURE 13. Nondimensionalized shear stress vs. nondimensionalized shear strain for fluid model.

PARTIAL-FILM EHL

Partial EHL is the regime where average film thickness becomes less than three times the composite surface roughness and the local film thickness is interrupted at the tip of tall asperities.[59] A majority of Hertzian contacts in gears, cams, and rolling element bearings operate in this regime.

For years, roughness of bearing surfaces has been characterized by a single parameter such as σ, the rms standard deviation of roughness amplitude from a mean plane. To supplement this indication of roughness, surface roughness texture can be described by two statistical parameters: height distribution and autocorrelation function, acf. For surfaces finished by an abrasive process, height distribution is approximately Gaussian.[60] For running-in surfaces, the height distribution is slightly skewed from Gaussian.

The acf measures the wave length structure of a surface profile in a given direction. It is defined as

$$R_x(\lambda) = \frac{1}{\ell} \int_0^{\ell} \delta(x) \cdot \delta\,(x + \lambda)dx \qquad (20a)$$

where λ is the correlation length, δ is the height function along the x-direction, and $R_x(\lambda)$ is the acf in the x-direction. The act for most engineering surfaces is an exponentially decaying function.[61] A linear function has been used as an approximation.[62]

Many engineering surfaces contain long wave lengths in one direction and short wave lengths in the normal direction. The pattern can be described by parameter γ defined as the ratio of x and y correlation lengths:[63]

$$\gamma = \frac{\lambda_{0.5\,x}}{\lambda_{0.5\,y}} \qquad (21)$$

Copyright © 1983 CRC Press LLC

where $\lambda_{0.5x}$ is the correlation length at which the acf of the profile is 50% of the value at the origin; γ may be interpreted as the length-to-width ratio of a representative asperity contact. Purely transverse, isotropic, and purely longitudinal roughness patterns have γ = 0,1,∞, respectively. Surfaces with $\gamma > 1$ are longitudinally oriented.

For determining partial EHL performance, surface roughness parameters required for each surface include: (1) σ — rms surface roughness, (2) height distribution function, (3)$\lambda_{0.5x}$, $\lambda_{0.5y}$ — 50% correlation lengths in x and y directions, and (4) acf (autocorrelation function).

Average Film Thickness

Pure longitudinal or transverse roughness was first explored by Johnson et al.[64] for pure rolling contact based on Christensen's stochastic theory.[65] They developed a Grubin type solution for $\sigma \ll h$ and concluded that the effect of roughness on average film thickness is minimal.

For $h/\sigma > 3$ and for rolling and sliding contacts, Berthè[66] and Chow and Cheng[67] showed that:

1. For pure rolling contact with pure transverse roughness, average film thickness is higher than predicted by smooth surface EHL theory. This effect is greatly enhanced as h/σ approaches three. For sliding contacts with one surface smoother than the other, the roughness effect is enhanced if the smoother surface is faster and retarded if the smoother surface is slower.
2. For pure longitudinal roughness, average film thickness is lower than predicted by the smooth surface theory. Superimposing of sliding on rolling has little influence on the roughness effect for pure longitudinal surfaces.

Patir and Cheng[62] developed an average flow model to handle roughnesses of an arbitrary surface pattern parameter γ and extended the results to h/σ below three where part of the load is shared by asperity contacts. Figure 14 depicts the flow pattern for longitudinally oriented ($\gamma > 1$), trasversely oriented ($\gamma < 1$), and isotropic roughness ($\gamma = 1$). In Figure 15, the ratio of actual film thickness to the smooth surface film thickness is plotted against film parameters $\Lambda = h_{smooth}/\sigma$.

Asperity Load to EHL Load Ratio

Average asperity contact pressure in partial EHL is a function of the ratio of compliance to composite surface roughness h/σ. Here, compliance is the distance between the two mean planes based on the underformed surfaces. For Gaussian surfaces, Tallian[59] has derived the asperity load as a function of h/σ for both plastically or elastically deformed asperities.

The load sharing ratios in circumferential ground EHL contacts (longitudinal roughness) can be obtained by a full numerical solution for disks with known surface roughness characteristics.[68]

Average Friction

Once the ratio of asperity load to fluid pressure load is determined, total friction force in partial EHL can be estimated by:

$$F = \mu_a Q_a + \mu_{EHL} Q_{EHL} \qquad (22)$$

where F = total frictional force, μ_a, μ_{EHL} = coefficient of friction for asperity load and hydrodynamic load, respectively, and Q_a,Q_{EHL} = asperity, hydrodynamic load. For most partial EHL contacts, μ_a is believed to be between 0.1 and 0.2. The value of μ_{EHL} can be taken from frictional coefficients for full-film EHL contacts.

Copyright © 1983 CRC Press LLC

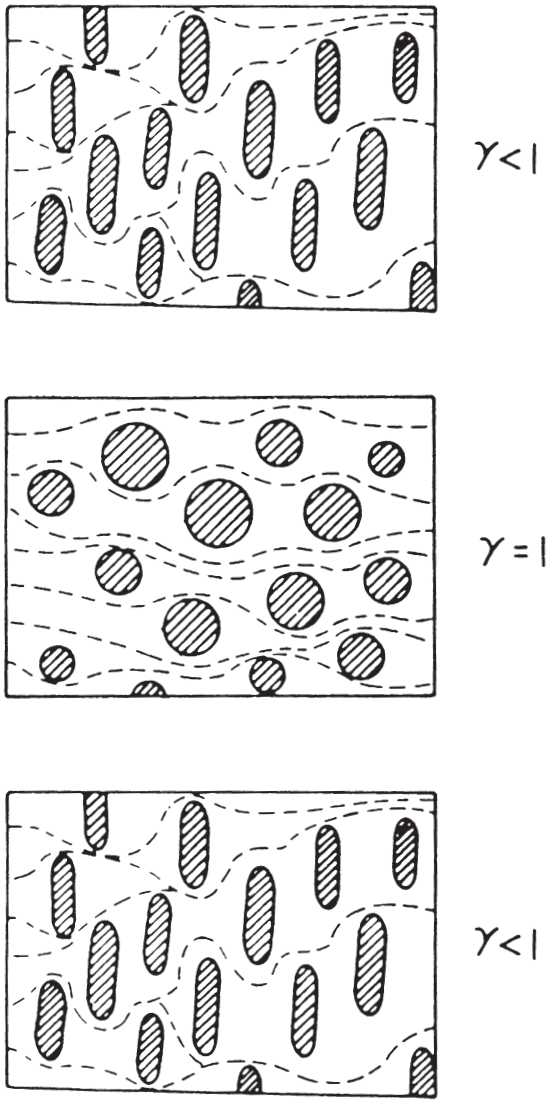

FIGURE 14. Typical contact area patterns for longitudinally oriented, isotropic, and transversely oriented rough surfaces.

Micro-Elastohydrodynamic Lubrication

Micro-EHL[69] deals with local pressure and film fluctuations around asperities or furrows within a macro-EHL conjunction. For pure rolling, local pressure and film thickness distributions at asperities are governed mainly by the normal approach action. As an ellipsoidal asperity approaches the opposing surface, the lubricant at the asperity center becomes highly pressurized and entrapped to form a central pocket as it travels through the Hertzian conjunction.[69,70]

For pure transverse ridges, the normal approach action in pure rolling causes the lubricant in the Hertzian region ahead of the asperity to become extremely viscous. Subsequently, the asperity becomes frozen together with the lubricant and is transported through the Hertzian conjunction as an integral unit.[71]

Copyright © 1983 CRC Press LLC

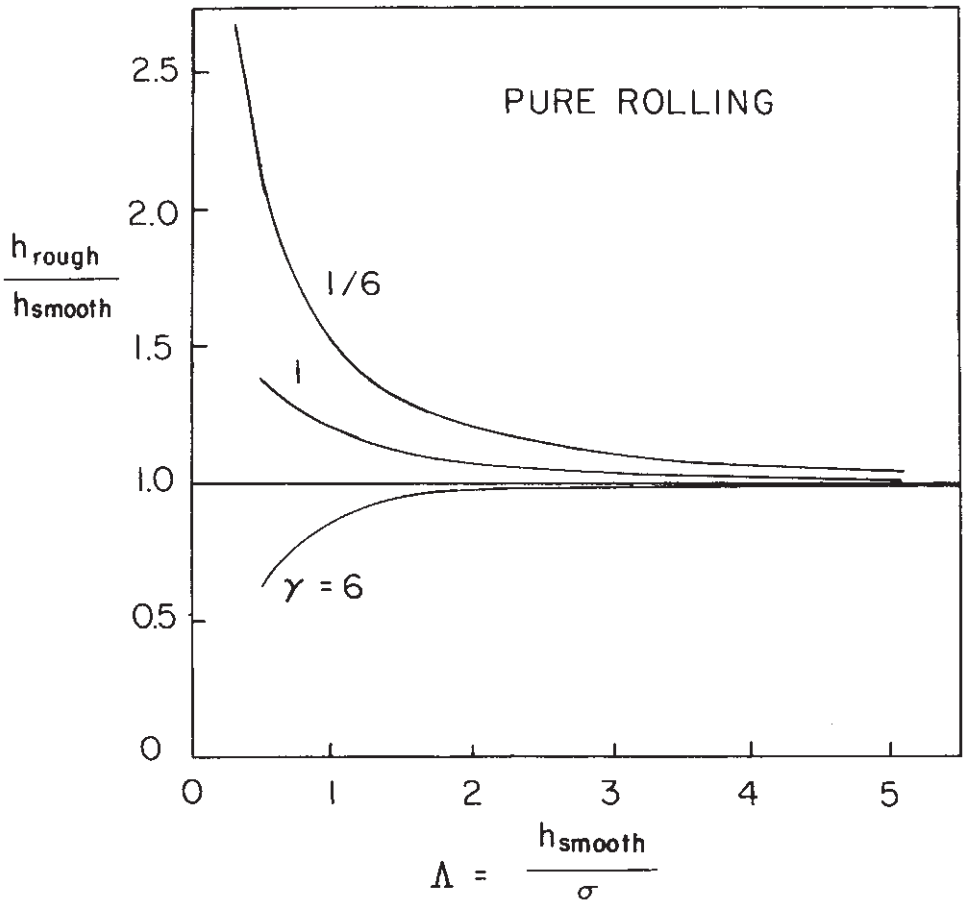

FIGURE 15. Effect of surface roughness on the average film thickness of EHL contacts: $P_o/E = 0.003$, pure rolling, $\alpha E = 3333$, and $\sigma/R = 1.8 \times 10^{-5}$.

For sliding EHL contacts, micro-EHL film thickness is controlled largely by entrainment of lubricant at the inlet of an asperity. For tranverse asperities, a lower limit of film thickness can be estimated by applying the classical EHL film thickness formulas to a sliding asperity in a low pressure ambient. For longitudinal asperities, very little is available to estimate minimum film thickness.

For a pair of transverse asperities colliding in a lubricant of low ambient pressure, micro-EHL film thickness can be estimated with existing theories.[72,73] If collision takes place in a high-pressure ambient, micro-EHL film is expected to increase considerably but cannot be predicted quantitatively.

COMPLIANT HYDRODYNAMIC JOURNAL AND THRUST BEARINGS

In hydrodynamic journal and thrust bearings, EHL effects can become significant if deformation of the bearing surfaces is of the same order as the film thickness. This occurs in heavily loaded journal bearings for large diesel engines, in high-pressure thrust bearings for hydroelectric turbines, and in elastomeric bearings used to tolerate dirt. Reference 74 gives a detailed review of compliant hydrodynamic bearings.

In journal bearings, minimum film thickness is increased slightly and peak film pressure is reduced when elastic effects are included. Surface deformations caused by local compres-

Copyright © 1983 CRC Press LLC

Table 2
VALUES OF C
FOR BEARING RACEWAYS

Bearing type	Inner race	Outer race
Ball	8.65×10^{-4}	9.43×10^{-4}
Spherical and cylindrical	8.37×10^{-4}	8.99×10^{-4}
Tapered and needle	8.01×10^{-4}	8.48×10^{-4}

Table 3
TYPICAL VALUES OF σ
FOR BEARINGS

	Composite roughness	
Bearing type	(μm)	(μin.)
Ball	0.178	7
Spherical and cylindrical	0.356	14
Tapered and needle	0.229	9

sion, bending of pads, and thermal distortion can significantly affect performance of large, high-speed thrust bearings.[75,76] Because deformation effects are sensitive to detailed pad geometry, they can only be determined by elaborate computer codes.[77]

APPLICATION TO MACHINE COMPONENTS

Based on EHL theories, effectiveness of lubrication in rolling element bearings,[3,78-81] gears,[3,78] and cams[82] can be calculated through the film parameter Λ, the ratio of film thickness to the composite surface roughness. In this section, formulas are taken mostly from an EHL guide book.[78]

Rolling Element Bearings

Roller bearings usually have line contacts and Equation 9 should be used to calculate film thickness. For ball bearings, contacts are elliptical with semimajor axis normal to the direction of rolling and Equations 10 through 13 should be used; to evaluate the speed and load parameter, rolling speed and contact dimensions must be determined from the geometry and kinematics of the system. Reference 78 gives formulas for all common commercial rolling bearings. A simplified film thickness formula, which does not involve detailed bearing geometry and yet gives an adequate prediction of film thickness, is given below:[78]

$$\Lambda = \frac{1}{\sigma} CD\,[LP \cdot N]^{0.74} \qquad (23)$$

where $\lambda = h/\sigma$, D = bearing outside diameter, m or in., C = a constant given in Table 2, dimensionless, $LP = \mu_o \alpha \cdot 10^{11}$, sec, μ_o = viscosity, N-sec/m^2 or lb-sec/in.^{2}, α = pressure-viscosity coefficient, m^2/N or in.^{2}/lb, N = difference between the inner and outer race speeds, rpm, h = film thickness in microns if D is in meters or in microinches if D is in inches, and σ = composite roughness, μm or μin. Typical values of α for bearings are given in Table 3.

An adequate λ for protecting bearing surfaces against early surface fatigue was shown to be greater than 1.5. Typical values of lubricant parameter, LP, for motor oils can be found in Figure 16.

Copyright © 1983 CRC Press LLC

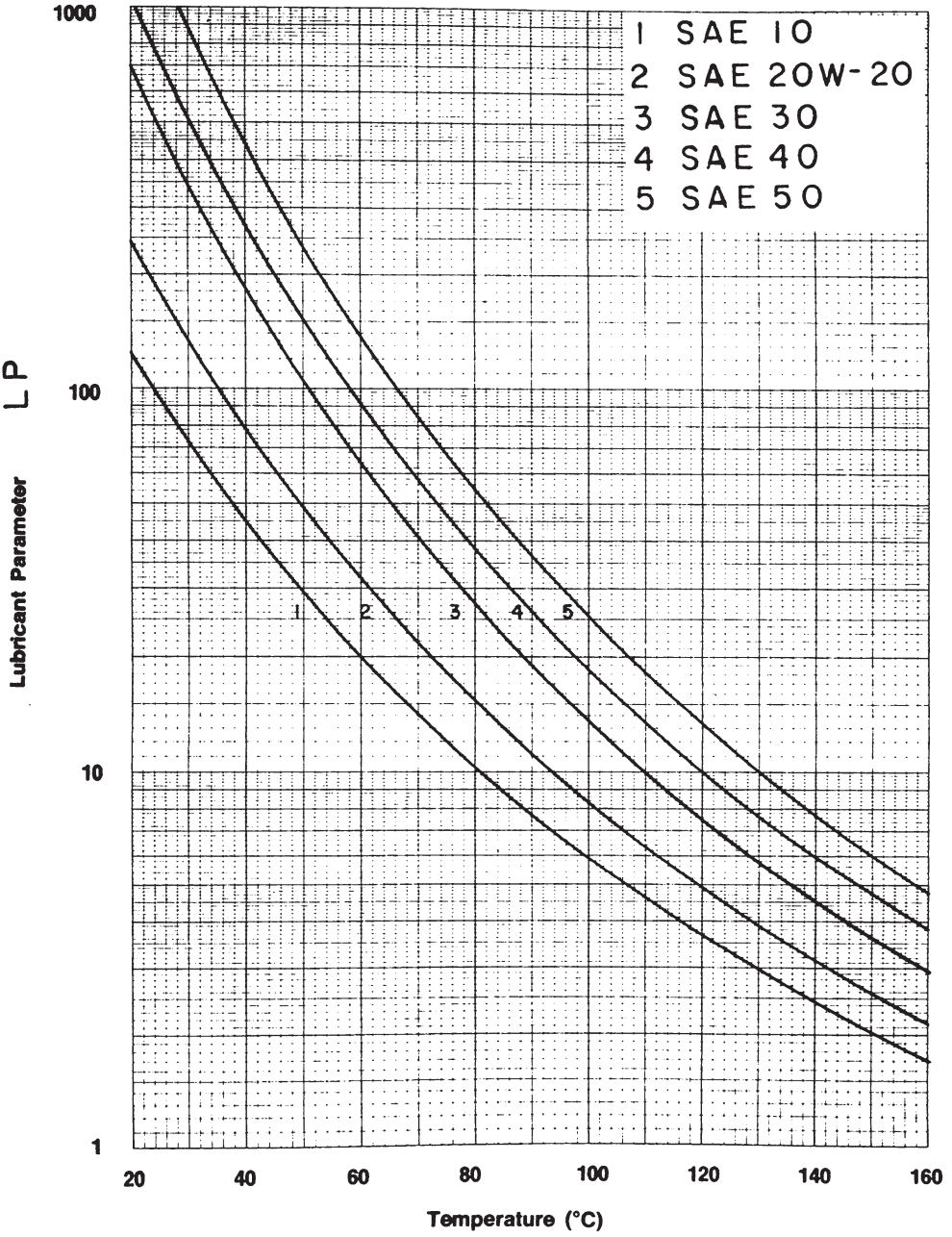

FIGURE 16. Typical value of the lubricant parameter LP.

Gears

Equation 24 is given here for calculating film parameter Λ in involute gears of the following types:

1. Internal and external, parallel, fixed axis spur, and helical gears.
2. Straight, zerol, and spiral bevel gears with any shaft angle.
3. Simple planetary gear trains.

Copyright © 1983 CRC Press LLC

Table 4
GEAR EQUATIONS

	Gear Type	N	G	W_T/ℓ	V	Notes
FIXED AXIS	Parallel Axis External	N_G	$\frac{3.4\times10^{-4}(m_G C\sin\phi_n)^{1.5}E_D^{0.148}}{(m_G+1)^2}$	$\frac{T_G(m_G+1)}{m_G CF\cos\phi_n\cos^2\psi}$	$\frac{2\pi m_G CN_G}{60(m_G+1)}$	Helical gears: Helix Angle = ψ Spur Gears: $\psi=0$
	Parallel Axis Internal	N_R	$\frac{3.4\times10^{-4}(m_G C\sin\phi_n)^{1.5}E_D^{0.148}}{(m_G-1)^2}$	$\frac{T_R(m_G-1)}{m_G CF\cos\phi_n\cos^2\psi}$	$\frac{2\pi m_G CN_R}{60(m_G-1)}$	
	Bevel Gear 90° Shaft Angle	N_G	$\frac{3.4\times10^{-4}(R_{Gm}\sin\phi_n)^{1.5}E_D^{0.148}}{(1+m_G^2)^{0.25}}$	$\frac{T_G}{R_{Gm}F\cos\phi_n\cos^2\psi_m}$	$\frac{2\pi R_{Gm}N_G}{60}$	Spiral bevels; Spiral angle = ψ_m
	Bevel with Shaft Angle Other than 90°	N_G	$\frac{3.4\times10^{-4}(R_{Gm}\sin\phi_n)^{1.5}E_D^{0.148}}{(\cos\gamma_G+m_G\cos\gamma_P)^{0.5}}$	$\frac{T_G}{R_{Gm}F\cos\phi_n\cos^2\psi_m}$	$\frac{2\pi R_{Gm}N_G}{60}$	Straight, Zerol. $\psi_m = 0$
PLANETARY	Sun-Planet	$\lvert N_S-N_C\rvert$	$3.4\times10^{-4}(R_S\sin\phi_n)^{1.5}\left(\frac{R_R-R_S}{R_R+R_S}\right)^{0.5}E_D^{0.148}$	$\frac{\lvert T_S\rvert}{nR_S F\cos\phi_n\cos^2\psi}$	$\frac{2\pi R_S}{60}\lvert N_S-N_C\rvert$	Helical gears: Helix Angle = ψ
	Ring-Planet	$\lvert N_R-N_C\rvert$	$3.4\times10^{-4}(R_R\sin\phi_n)^{1.5}\left(\frac{R_R-R_S}{R_R+R_S}\right)^{0.5}E_D^{0.148}$	$\frac{\lvert T_R\rvert}{nR_R F\cos\phi_n\cos^2\psi}$	$\frac{2\pi R_R}{60}\lvert N_R-N_C\rvert$	Spur gears: $\psi = 0$

Note: Where:

$\lVert$	=	Absolute (positive) value	N_g	=	gear wheel speed, rpm	T_s	=	sun gear torque
C	=	Center distance	N_R	=	ring gear speed, rpm	T_R	=	ring gear torque
E_D	=	reduced modulus (equation 2)	N_s	=	sun gear speed, rpm	γ_G	=	gear cone angle
F	=	face width	R_{Gm}	=	midface pitch radius	γ_P	=	pinion cone angle
m_G	=	gear ratio	R_R	=	ring gear radius	ϕ_n	=	normal pressure angle
n	=	Number of planets	R_s	=	sun gear radius	ψ	=	helix angle
N_c	=	Carrier speed, rpm	T_G	=	gear wheel torque	ψ_m	=	midface spiral angle

Table 5
TYPICAL VALUES OF COMPOSITE ROUGHNESS, σ

	Initial value		Run-In value	
Tooth finish	**μm**	**μin.**	**μm**	**μin.**
Hobbed	1.78	70	1.02	40
Shaved	1.27	50	1.02	40
Ground soft	0.89	35	—	—
Ground hard	0.51	20	—	—
Polished	0.18	7	—	—

$$\Lambda = \frac{1}{\sigma}\left[G\,LP\,N\left(\frac{W_T}{\ell}\right)^{-0.148}\right]^{0.74} \qquad (24)$$

where G = geometrical parameter from Table 4, LP = $\mu_o\alpha\cdot10^{11}$, sec, N = gear rotational speed, rpm, W_τ/ℓ = load per unit length of contact from Table 4, and σ; = composition roughness, see Table 5.

Copyright © 1983 CRC Press LLC

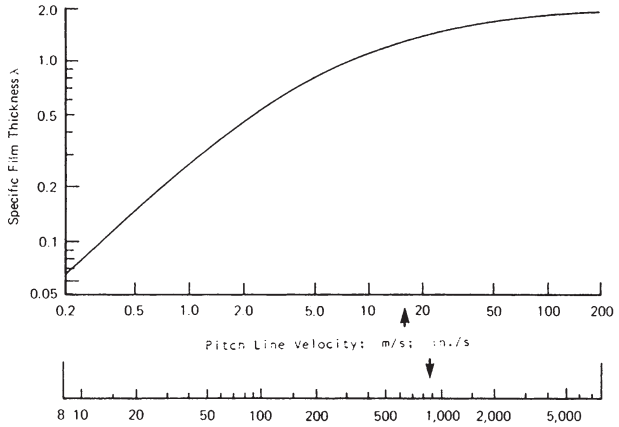

FIGURE 17. Adjusted specific film thickness vs. pitch line velocity (5% probability of distress).

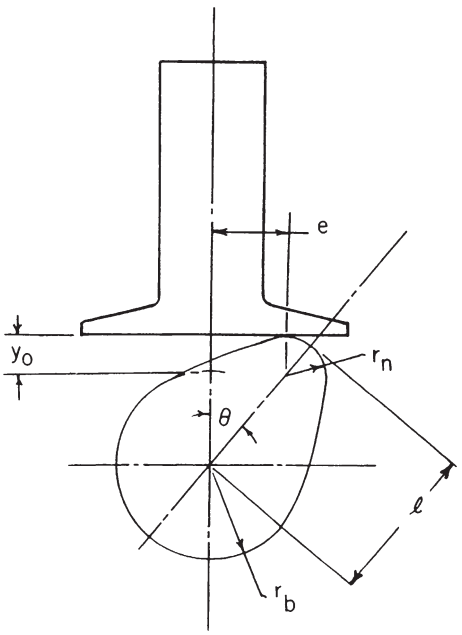

FIGURE 18. Geometry of a cam-follower contact.

The critical value of Λ at which a 5% probability of surface distress is expected is an empirical function of pitch line velocity V as shown in Figure 17. Equations for V for different types of gears are given in Table 4.

Cam-Follower Systems

The film parameter Λ for a cam-flat follower Figure 18 system can be calculated by Equation 25:

$$\Lambda = \frac{1}{\sigma} 4.35 \times 10^{-3} \left[f_N \, LP \, N \right]^{0.74} R^{0.26} \qquad (25)$$

Copyright © 1983 CRC Press LLC

where N = cam shaft speed, rpm, LP = lubricant parameter, sec, $f_N = |2r_n - \ell|$, where ℓ is the distance from the nose tip to the shaft axis and r_n is the nose radius (see Figure 18), m or in., $R = (1/r_n + 1/r_f)^{-1}$, m or in., r_n = nose radius, m or in., r_f = follower radius, m or in., and σ = composite roughness, μm or μin.

In general, Λ in cam systems is well below one. In this regime, EHL is ineffective and one must rely heavily on surface film or boundary lubrication to protect surfaces against scuffing and wear.

REFERENCES

1. **Martin, H. M.,** Lubrication of gear teeth, *Engineering (London),* 102, 199, 1916.
2. **Grubin, A. N.,** Contact stresses in toothed gears and worm gears, *Central Scientific Research Institute for Technology and Mechanical Engineering,* Book No. 30., Moscow. (D..S.I..R. English Translation No. 337. As communicated by Prof. M. M. Krushchov to Prof. A. Cameron, Grubin's contribution was originally studied by A. M. Ertel and after his death was seen ihrough the press by his co-worker Grubin and is thus often known as Grubin's name alone.)
3. **Dowson, D. and Higginson, G. R.,** *Elastohydrodynamic Lubrication,* Pergamon Press, Oxford, 1977.
4. **Cheng, H. S.,** Isothermal EHD theory for the full range of pressure-viscosity coefficient, *J. Lubr. Technol. Trans. ASME,* 94(1), 35, 1972.
5. **Ford, R. A. J.,** The Lubrication of High Speed Gas Turbine Roller Bearings, Ph.D. thesis, University of London, March, 1975.
6. **Greenwood, J. and Kanzlarich, J.,** Inlet shear heating in elastohydrodynamic lubrication, *J. Lubr. Technol. Trans. ASME,* 95(4), 417, 1973.
7. **Cheng, H. S.,** *Calculation of Elastohydrodynamic Film Thickness in High-Speed Rolling and Sliding Contacts,* Rep. No. MTI-67TR24, Mechanical Technology Inc., Latham, N.Y., May 1967.
8. **Murch, L. E. and Wilson, W. R. D.,** A thermal elastohydrodynamic inlet zone analysis, *J. Lubr. Technol., Trans. ASME,* 97(2), 212, 1975.
9. **Wolveridge, P. E., Baglin, K. P., and Archard, J. F.,** The starved lubrication of cylinders in line contact, Proc. Inst. Mech. Eng., 185, 1159, 1970.
10. **Dowson, D., Saman, W. Y., and Toyoda, S.,** A study of starved elastohydrodynamic line contacts, *Proc. 5th Leeds-Lyon Symp. Tribology,* Leeds, England, 1979.
11. **Archard, J. F.,** Experimental studies of elastohydrodynamic lubrication, *Proc. Inst. Mech. Eng.,* 180(38), 17, 1965.
12. **Crook, A. W.,** The lubrication of rollers. II. Film thickness with relation to viscosity and speed, *R. Soc. London Philos. Trans. Ser. A,* 254, 223, 1961.
13. **Sibley, L. B. and Orcutt, F. K.,** Elastohydrodynamic lubrication of rolling contact surfaces, *Am. Soc. Lubr. Eng. Trans.,* 4(2), 234, 1961.
14. **Wymer, D. G. and Cameron, A.,** EHD lubrication of a line contact, *Proc Inst. Mech. Eng.,* 188, 221, 1974.
15. **Dowson, D. and Higginson, G. R.,** A numerical solution to the elastohydrodynamic problem, *J. Mech. Eng. Sci.,* 1(1), 6, 1959.
16. **Dowson, D., Higginson, G. R., and Whitaker, A. V.,** Elastohydrodynamic Lubrication — a survey of isothermal solutions, *J. Mech. Eng. Sci.,* 4(2), 121, 1962.
17. **Archard, G. D., Gair, F. C., and Hirst, W.,** The elastohydrodynamic lubrication of rollers, *Proc. R Soc. London Ser. A,* 262, 51, 1961.
18. **Hamilton, G. M. and Moore, S. L.,** Deformation and pressure in an EHD contact, *Proc. R. Soc. London Ser. A,* 322, 313, 1971.
19. **Rodkiewicz, C. M. and Srinivanasan, V.,** EHD lubrication in rolling and sliding contacts, *J. Lubr. Technol. Trans. ASME,* 94(4), 324, 1972.
20. **Rohde, S. M.,** A unified treatment of thick and thin film EHD problems by using high order element methods, *Proc. R. Soc. London Ser. A,* 343, 315, 1975.
21. **Dowson, D.,** Elastohydrodynamic Lubrication, Interdisciplinary Approach to the Lubrication of Concentrated Contacts, Spec. Publ. No. NASA SP-237, National Aeronautics and Space Administration, Washington, D.C., 1970, 34.
22. **Kannel, J. W. et al.,** A Study of the Influence of Lubricants on High-Speed Rolling-Contact Bearing Performance, Part IV, Tech. Rep. No. ASD-TR-61-643, Air Force Aero Propulsion Laboratory, Dayton, Ohio. 1964.

Copyright © 1983 CRC Press LLC

23. **Gohar, R. and Cameron, A.,** The mapping of F.HD contacts, *ASLE Trans.,* 10, 214, 1967.
24. **Orcutt, F. K.,** Experimental study of elastohydrodynamic lubrication, *ASLE Trans.,* 8, 381, 1965.
25. **Kannel, J. W.,** The measurement of pressure in rolling contacts, *Proc. Inst. Mech. Eng.,* 180(3B), 135, 1965.
26. **Moes, I. H.,** Communications to EHL symposium held at Leeds University, *Proc. Inst. Mech. Eng.,* 180(3B), 244, 1965.
27. **Herrebrugh, K.,** Solving the incompressible and isothermal problem in elastohydrodynamic lubrication through an integral equation, *J. Lubr. Technol., Trans. ASME,* 90(1), 262, 1968.
28. **Archard, J. F. and Cowking, E. W.,** A simplified treatment of elastohydrodynamic lubrication theory for a point contact, *Proc. inst. Mech. Eng.,* 180(3B), 47, 1965.
29. **Cheng, H. S.,** A numerical solution of the elastohydrodynamic film thickness in an elliptical contact, *J. Lubr. Technol., Trans. ASME,* 92(1), 155, 1970.
30. **Hamrock, B. J. and Dowson, D.,** Isothermal elastohydrodynamic lubrication of point contacts, *J. Lubr. Technol.,* 98(2), 223, 1976; 98(3), 1976; 99(2), 264, 1977; 99(1), 15, 1977.
31. **Chiu, Y. P.,** An analysis and prediction of lubricant film starvation in rolling contact systems, *ASLE Trans.,* 17, 22, 1974.
32. **Chiu, Y. P. et al.,** *Exploratory Analysis of EHD Properties of Lubricants,* Rep. No. AL72P10. SKF Industries, King of Prussia, Pa., 1972.
33. **Snidle, R. W. and Archard, J. F.,** Experimental investigation of elastohydrodynamic lubrication at point contacts, *Proc. 1972 Symp. Elasiohydrodynamic Lubrication,* Paper C2/72, Institute of Mechanical Engineers, London, 1972, 5.
34. **Wedevan, L. D.,** Optical Measurements in EHD Rolling-Contact Bearings, Ph.D. thesis. University of London, March 1970.
35. **Westlake, F. J. and Cameron, A.,** Interferomatric study of point contact lubrication, *Proc. 1972 Symp. Elastohydrodynamic Lubrication,* Paper C39/72, Institute of Mechanical Engineers, London, 1972, 153.
36. **Sanborn, D. M. and Winer, W. O.,** Fluid rheological effects in sliding elastohydrodynamic point contacts with transient loading. I. Film thickness, *J. Lubr. Technol., Trans. ASME,* 93(2), 262, 1971.
37. **Parker, R. J. and Kannel, J. W.,** EHD Film Thickness Between Rolling Discs with a Synthetic Paraffinic Oil to 589 K, NASA Tech. Note D-6411, National Aeronautics and Space Administration, Washington, DC, 1970.
38. **Gentle, C. R., Duckworth, R. R., and Cameron, A.,** EHD Film thickness at extra pressures, *J. Lubr. Technol., Trans. ASME,* 97, 383, 1975.
39. **Hirst, W. and Moore, A. J.,** Elastohydrodynamic Lubrication at High Pressures, Tech. Rep., University of Reading, Reading, U.K., 1977.
40. **Foord, C. A. et al.,** Optical elastohydrodynamics, *Proc. Inst. Mech. Eng.,* 184(1), 487, 1969.
41. **Jacobson, B.,** On the lubrication of heavily loaded spherical surfaces considering surface deformations and solidification of the lubricant, *Acta Polytechn. Scand. Mech. Eng. Ser.,* 54, 1970.
42. **Ranger, A. P.,** Numerical Solutions to the EHD Problems, Ph.D. thesis, University of London, March, 1974.
43. **Cheng, H. S. and Sternlicht, B.,** A numerical solution for pressure, temperature and film thickness between two infinitely long rolling and sliding cylinders under heavy load, *J. Basic Eng., Trans. ASME.* 87(3), 695, 1965.
44. **Dowson, D. and Whittaker, B. A.,** A numerical procedure for the solution of the elastohydrodynamic problem of rolling and sliding contacts lubricated by a newtonian fluid, *Proc. Inst. Mech. Eng.,* 180(3B), 57, 1965.
45. **Kannel, J. W. and Bell, J. C.,** A method for estimating of temperature in lubricated rolling-sliding gear or bearing EHD contacts, Paper C24/72, *Proc. 1972 Symp. Elastohydrodynamic Lubrication,* Institute of Mechanical Engineers, London, 1972, 118.
46. **Kannel, J. W., Zugaro, F. F., and Dow, T. A.,** A method for measuring surface temperature between rolling/sliding steel cylinders, *J. Lubr. Technoi. Trans. ASME,* 100(1), 100, 1978.
47. **Nagaraj, H. S., Sanborn, D. M., and Winer, W. O.,** Direct surface temperature measurement by infrared radiation in elastohydrodynamic contacts and the correlation with the Block temperature theory, *Wear,* 49, 1, 1978.
48. **Jaeger, J. C.**, Moving sources of heat and the temperature at sliding contacts, *Proc. R. Soc. N.S.W.,* 56, 203, 1942.
49. **Johnson, K. L. and Cameron, R.,** Shear behavior of elastohydrodynamic oil film at high rolling contact pressures, *Proc. Inst. Mech. Eng.,* 182, 307, 1967.
50. **Harrison, G. and Trachman, E. G.,** The role of compressional viscoelasticity in the lubrication of rolling contacts, *J. Lubr. Technol., Trans. ASME,* 95, 306, 1972.
51. **Dyson, A.,** Frictional traction and lubricant rheology in elastohydrodynamic lubrication, *Philas. Trans. R. Soc. London,* 266, 1170, 1970.

Copyright © 1983 CRC Press LLC

52. **Johnson, K. L. and Tevaariverk, J. L.,** Shear behavior of EHD oil films, *Proc. R. Soc. London,* A356, 215, 1977.
53. **Barlow, A. J. et al.,** The effect of pressure on the viscoelastic properties of liquids, *R. Soc. London Proc.,* A327, 403, 1972.
54. **Montrose, C. J., Moynihan, C. T., and Sasake, H.,** Dynamic Shear and Structural Viscoelasticity in EHD Lubrication, Vitreous State Laboratory Tech. Rep., July 1977.
55. **Bell, J. C.,** Lubrication of rolling surfaces by a Ree-Eyring fluid, *ASLE Trans.,* 5, 160, 1962.
56. **Trachman, E. and Cheng, H. S.,** Thermal and non-Newtonian effects on traction in elastohydrodynamic lubrication, Paper C37/72, *Proc. 1972 Syrnp. Elastohydrodynamic Lubrication,* Insfitute of Mechanical Engineers, London, 1972, 142.
57. **Smith, F. W.,** Rolling contact lubrication — the application of elastohydrodynamic theory, *J. Lubr. Technol., Trans. ASME Ser. D,* 87, 170, 1965.
58. **Bair, S. and Winer, W. O.,** A theological model for EHD contacts based on primary laboratory data, *J. Lubr. Technol., Trans. ASME,* 101(3), 258, 1979.
59. **Tallian, T. E.,** The theory of partial elastohydrodynamic contacts, *Wear,* 21, 49, 1972.
60. **Williamson, J. B. P.,** Topography of solid surfaces, in *Interdisciplinary Approach to Friction and Wear,* NASA SP-181. National Aeronautics and Space Administration, Washington, D.C., 1968, 143.
61. **Whitehouse, D. J. and Archard, J. F.,** The properties of random surfaces of significance in their contact, *Proc. R. Soc. London,* A316, 97, 1970.
62. **Patir, N. and Cheng, H. S.,** An average flow model for determining effects of three dimensional roughness on partial hydrodynamic lubrication, *J. Lubr. Technol., Trans. of ASME,* 100(1), 12, 1978.
63. **Feblenik, J.,** New developments in surface characterization and measurement by means of random process analysis, *Proc. Inst. Mech. Eng.,* 182(3K), 108. 1967.
64. **Johnson, K. L., Greenwood, J. A., and Poon, S. Y.,** A simple theory of asperity contact in elastohydrodynamic lubrication, *Wear,* 19, 1972, 91.
65. **Christensen, H.,** Stochastic models for hydrodynamic lubrication of rough surfaces, *Proc. Inst. Mech. Eng. Tribology Group,* 184(1,55), 1013, 1969.
66. **Berthè, D.,** Les Effects Hydrodynamiques Sur La Fatigue Des Surfaces Dans Les Contacts Hertziens,D. Sc. thesis, University of Lyon, France, 1974.
67. **Chow, L. S. H. and Cheng, H. S.,** The effect of surface roughness on the average film thickness between lubricated rollers, *J. Lubr. Technol., Trans. ASME,* 98(1), 117, 1976.
68. **Cheng, H. S. and Dyson, A.,** Elastohydrodynamic lubrication of circumferentially ground disks, *ASLE Trans.,* 21(1), 25, 1978.
69. **Cheng, H. S.,** On some aspects of micro-elastohydrodynamic lubrication, *Proc. 4th Leeds-Lyon Symp. Lubr.,* April 1977.
70. **Christensen, H.,** Elastohydrodynamic theory of spherical bodies in normal approach motion, *J. Lubr. Tech., Trans. ASME,* 92, 145, 1970.
71. **Lee, K. M. and Cheng, H. S.,** The Effect of Surface Asperity on the Elastohydrodynamic Lubrication, NASA CR-2195, National Aeronautics and Space Administration, Washington, D.C., 1973.
72. **Fowles, P. E.,** The application of elaslohydrodynamic theory to individual asperity-asperity collisions, *J. Lubr. Tech., Trans. ASME,* 91, 464, 1969.
73. **Fowles, P. E.,** A thermal elastohydrodynamic theory for individual asperity-asperity collision, *J. Lubr. Tech., Trans. ASME,* 93, 383, 1971.
74. **Rohde, S.,** Thick film and transient elastohydrodynamic lubrication problems, *Proceedings on Fundamentals of Tribology.* MIT Press, Cambridge, Mass., 1979.
75. **Castelli, V. and Malanowski, S. B.,** Method for solution of lubrication problems with temperature and elasticity effects: Application to sector, tilting-pad bearings, *J. Lubr. Technol. Trans. ASME,* 91(4), 634, 1969.
76. **Taniguichi, S. and Ettles, C.,** A thermal elastic analysis of the parallel surface thrust washer, *ASCE Trans.,* 18(4), 299, 1975.
77. **Ettles, C.,** The development of a generalized computer analysis for sector shaped tilting pad thrust bearings**,** *ASLE Trans.,* 19(2), 153, 1976.
78. **Anon.,** *EHL Guidebook,* Mobile Oil Corporation. New York, 1979.
79. **McGrew, J. M. et al.,** Elastohydrodynamic Lubrication — Preliminary Design Manual, Tech. Rep. AFAPL-TR-70-27, Air Force Propulsion Laboratory, Dayton, Ohio, 1970.
80. **Cheng, H. S.,** *Application of Elastohydrodynamics of Rolling Element Bearings,* ASME Paper 74-DE-32, American Society of Mechanical Engineers, New York, 1974.
81. **Anon.,** *SKE Engineering Data,* SKF Industries, Inc., King of Prussia, Pa., 1968.
82. **Dyson, A.,** Discussion of "Elastohydrodynamic Lubrication" by D. Dowson, Spec. Publ. SP-237, National Aeronautics and Space Administration, Washington, D.C., 1970.
83. **Orcutt, F. K. and Cheng, H. S.,** Lubrication of rolling contact instrument bearings, gyro spin-axis, *Hydrodynamic Bearing Symp.,* Vol. 2, M.I.T. Instrument Laboratory, Cambridge, Mass., 1966.

Copyright © 1983 CRC Press LLC